

A search for linear polarization in the active galactic nucleus 3C 84 at 239 and 348 GHz^{*}

S. Trippe¹†, M. Bremer², T. P. Krichbaum³, M. Krips², R. Neri², V. Piétu²,
J. M. Winters²

¹*Seoul National University, Department of Physics and Astronomy, 599 Gwanak-ro, Gwanak-gu, Seoul 151-742, South Korea*

²*Institut de Radioastronomie Millimétrique (IRAM), 300 rue de la Piscine, F-38406 Saint Martin d'Hères, France*

³*Max-Planck-Institut für Radioastronomie, Auf dem Hügel 69, D-53121 Bonn, Germany*

Accepted 2012 June 9. Received 2012 June 8; in original form 2012 March 30

ABSTRACT

We report a search for linear polarization in the active galactic nucleus (AGN) 3C 84 (NGC 1275) at observed frequencies of 239 GHz and 348 GHz, corresponding to rest-frame frequencies of 243 GHz and 354 GHz. We collected polarization data with the IRAM Plateau de Bure Interferometer via Earth rotation polarimetry. We do not detect linear polarization. Our analysis finds 3σ upper limits on the degree of polarization of 0.5% and 1.9% at 239 GHz and 348 GHz, respectively. We regard the influence of Faraday conversion as marginal, leading to expected circular polarizations $\leq 0.3\%$. Assuming depolarization by a local Faraday screen, we constrain the rotation measure, as well as the fluctuations therein, to be $\geq 10^6 \text{ rad m}^{-2}$. From this we estimate line-of-sight magnetic field strengths of $\geq 100 \mu\text{G}$. Given the physical dimensions of 3C 84 and its observed structure, the Faraday screen appears to show prominent small-scale structure, with $\Delta\text{RM} \geq 10^6 \text{ rad m}^{-2}$ on projected spatial scales $\leq 1 \text{ pc}$.

Key words: galaxies: active — galaxies: ISM — galaxies: individual: 3C 84 (NGC 1275) — polarization — radiation mechanisms: non-thermal — techniques: polarimetric.

1 INTRODUCTION

At radio frequencies, active galactic nuclei (AGN) are luminous emitters of synchrotron radiation (see, e.g., Krolik (1999), or Kembhavi & Narlikar (1999), for reviews). Radio observations of AGN find degrees of linear polarizations in the range $\approx 1\text{--}20\%$ with a mean value of about $\approx 5\%$ (Altschuler & Wardle (1976; 1977); Aller et al. (1985); Nartallo et al. (1998); Trippe et al. (2010); Agudo et al. (2010)). Linear polarization provides information on physical parameters of emitters like emission region structure, geometry and strengths of magnetic fields, and particle densities (e.g., Saikia & Salter (1988), and references therein). Accordingly, studies of their polarized light deepen the understanding of the physics of active galaxies.

The active nucleus of the Seyfert 2 galaxy 3C 84 (NGC 1275), located at a redshift $z=0.018$, is known for its highly unusual radio polarization properties. Linear polarization has been found on levels consistently lower than 1% at frequencies from 5 GHz to 43 GHz¹. Radio-interferometric maps obtained with the Very Long

Baseline Array (VLBA) at 15 GHz, providing angular resolutions of ≈ 2 milliseconds of arc, unveil linear polarization on levels $\leq 8\%$ within a small region less than about one parsec in size (Taylor et al. (2006))². Additionally, 3C 84 shows substantial *circular* polarization with degrees of circular polarization being $\approx 0.2\text{--}3\%$ depending on frequency and angular resolution (Aller et al. (2003); Homan & Wardle (2004); Agudo et al. (2010)). The combination of low linear and high circular polarization indicates efficient Faraday depolarization (e.g., Dreher et al. (1987)) and Faraday conversion (e.g., Jones (1988)) by matter surrounding the nucleus. Accordingly, Taylor et al. (2006) identify ionized gas permeated by magnetic fields with substructure on scales $\leq 10 \text{ pc}$ as Faraday screen.

Given the state of the art, a detection and analysis of linear polarization in 3C 84 may be achieved via two roads. First, high angular resolution mapping is apparently able to separate high and low polarization regions spatially and reduce the “masking” of polarized flux by spatial averaging in telescope beams. Second, observations at high (sub-)millimetre radio frequencies should be less af-

^{*} This study is based on observations carried out with the IRAM Plateau de Bure Interferometer. IRAM is supported by INSU/CNRS (France), MPG (Germany), and IGN (Spain).

† E-mail: trippe@astro.snu.ac.kr

¹ According to, e.g., monitoring results from the Effelsberg radio observatory (U. Bach, MPIfR Bonn, priv.

comm.) or the Very Large Array calibration data base (<http://www.aoc.nrao.edu/~smyers/calibration/master.shtml>).

² See also, e.g., the data bases of the MOJAVE survey (Lister et al. (2009); <http://www.physics.purdue.edu/astro/MOJAVE/sourcepages/0316+413.shtml>) or the University of Michigan Radio Astronomy Observatory (<http://www.astro.lsa.umich.edu/obs/radiotel/umrao.php>).

ected by Faraday depolarization than previous observations aimed at lower frequencies. This is a consequence of the fact that the strength of Faraday depolarization, and thus the loss of linear polarization, is proportional to the square of the rest-frame wavelength λ_0^2 .

In this article we report the results of observations with the IRAM Plateau de Bure Interferometer (PdBI; Winters & Neri (2011)³) at 239 GHz and 348 GHz. We followed the high-frequency approach outlined above in order to detect the linear polarization of 3C 84 without resolving the source spatially.

2 OBSERVATIONS AND DATA ANALYSIS

The Plateau de Bure Interferometer is composed of six antennas with 15 m diameter each. All antennas are equipped with dual linear polarization Cassegrain focus receivers. Both orthogonal linear polarizations – “horizontal” (H) and “vertical” (V) with respect to the antenna frame – are observed simultaneously. Observations can be carried out (non-simultaneously) in four atmospheric windows located around wavelengths of 0.8 mm, 1.3 mm, 2 mm, and 3 mm. Each of these bands covers a continuous range of frequencies. Frequency ranges are 277–371 GHz for the 0.8-mm band, 201–267 GHz for the 1.3-mm band, 129–174 GHz for the 2-mm band, and 80–116 GHz for the 3-mm band. Within a given band, any frequency is available for observations.

At the time of the observations presented here, the PdBI was not yet equipped for observations of all Stokes parameters. We obtained linear polarization data via Earth rotation polarimetry, i.e. by monitoring the fluxes in the H and V channels as functions of parallactic angle ψ . For deriving the polarization of a source, we calculate the parameter

$$q(\psi) = \frac{V - H}{V + H}(\psi) = \frac{Q}{I} \cos(2\psi) + \frac{U}{I} \sin(2\psi) \quad (1)$$

from the fluxes $H(\psi)$ and $V(\psi)$. Here I , Q , and U are the relevant Stokes parameters. The second equality means that $q(\psi)$ provides full information on linear polarization (see, e.g., Sault, Hamaker & Bregman (1996); Thompson, Moran & Swenson (2001); but also Beltrán et al. (2004)) if a sufficient range of ψ is observed.

Due to the nature of polarized light and the fact that the PdBI antenna receivers are located in the Cassegrain foci, observing a polarized target results in $q(\psi)$ being a cosinusoidal signal with a period of 180° . The functional form of $q(\psi)$ is thus

$$q(\psi) \equiv m_L \cos [2(\psi - \chi)] \quad (2)$$

Here m_L is the fraction of linear polarization (ranging from 0 to 1; in the following, we will express m_L in units of %) and χ is the polarization angle (ranging from 0° to 180°). A more detailed discussion of the methodology is provided in Trippe et al. (2010).

As stated by Eq. 1, $q(\psi)$ is a relative parameter and therefore not affected by inaccuracies of flux or gain calibrations – equal factors multiplied to H and V cancel out. Accordingly, fluctuations of gain or atmospheric opacity do not affect $q(\psi)$ systematically. Equally, we do not require a dedicated calibration of amplitude or flux scales. However, we identify two sources of systematic errors we need to address before proceeding with the analysis (see also the corresponding discussion in Trippe et al. (2010)).

First, we may expect a certain level of instrumental polarization. As for the PdBI, the receivers are located in the Cassegrain

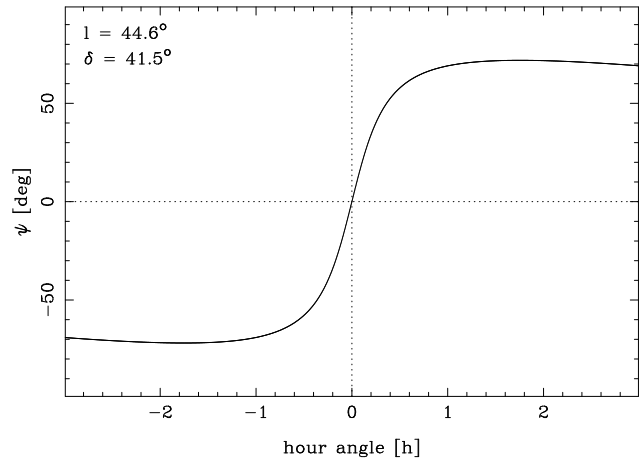


Figure 1. Parallactic angle ψ (in units of degrees) vs. hour angle (in units of hours) for 3C 84 as observed from the latitude of the PdBI. The source declination is $\delta = 41.5^\circ$, the latitude of the observatory is $l = 44.6^\circ$.

foci of the antennas. Accordingly, the instrumental polarization signal is fix with respect to the antenna, whereas the astronomical polarization signal is fix with respect to the sky. In terms of $q(\psi)$, astronomical polarization introduces a cosinusoidal dependence on ψ as stated by Eq. 2. Instrumental polarization contributes a constant offset o , meaning we effectively deal with a modified polarization model

$$q(\psi) \longrightarrow q'(\psi) = m_L \cos [2(\psi - \chi)] + o \quad (3)$$

The exact value of instrumental polarization is not well known for the PdBI. Trippe et al. (2010) were able to probe the behaviour of the PdBI receivers in the frequency range 84–116 GHz by means of laboratory experiments. For this frequency range, they found receiver polarizations of $\sim 0.3\%$. However, astronomical and instrumental polarization appear as separate parameters in Eq. 3. This means that instrumental polarization is not able to modify the values we observe for m_L in a systematic fashion. However, this statement does not hold entirely if instrumental polarization is a function of antenna orientation; we discuss this effect in detail in Sect. 3.

Second, there may be systematic differences in the gains, or efficiencies, of the H and V channels. If this is the case, one can rewrite the H channel flux as $H(\psi) \rightarrow rH(\psi)$ with $r > 0$ being the ratio of the gains of channels H and V. Any $r \neq 1$ modifies $q(\psi)$ such that (1) the mean value of $q(\psi)$ differs from zero, and (2) the polarization amplitude m_L is slightly reduced. Effect (1) is absorbed by the parameter o in Eq. 3. Effect (2) is very small even for large $r = 0.8 \dots 1.2$. As one can easily evaluate numerically, such gain ratios lead to a relative reduction of degrees of polarization m_L by $\approx 1\%$ at most. This means that for a source with a physical $m_L = 1\%$ we would actually measure $m'_L = 0.99\%$ – an effect we may safely ignore. Eventually, we conclude that both, instrumental polarization as well as gain differences, are kept under control by use of polarization model $q'(\psi)$ (Eq. 3).

We observed 3C 84 on 9 March 2011 at a frequency of 348 GHz and on 11 March 2011 at 239 GHz. We recorded source fluxes in cycles of 15 minutes composed of 30 adjacent “scans” of 30 seconds duration each. Each scan is divided further into 30 “dumps” of one second duration each. Between two consecutive cycles, pointing and focus of the antennas were checked and adjusted if necessary, using 3C 84 as reference point source; these calibration intervals took between three and seven minutes of time. Accurate Earth rotation polarimetry requires a good coverage in

³ <http://www.iram.fr/IRAMFR/GILDAS/doc/pdf/pdbi-intro.pdf>

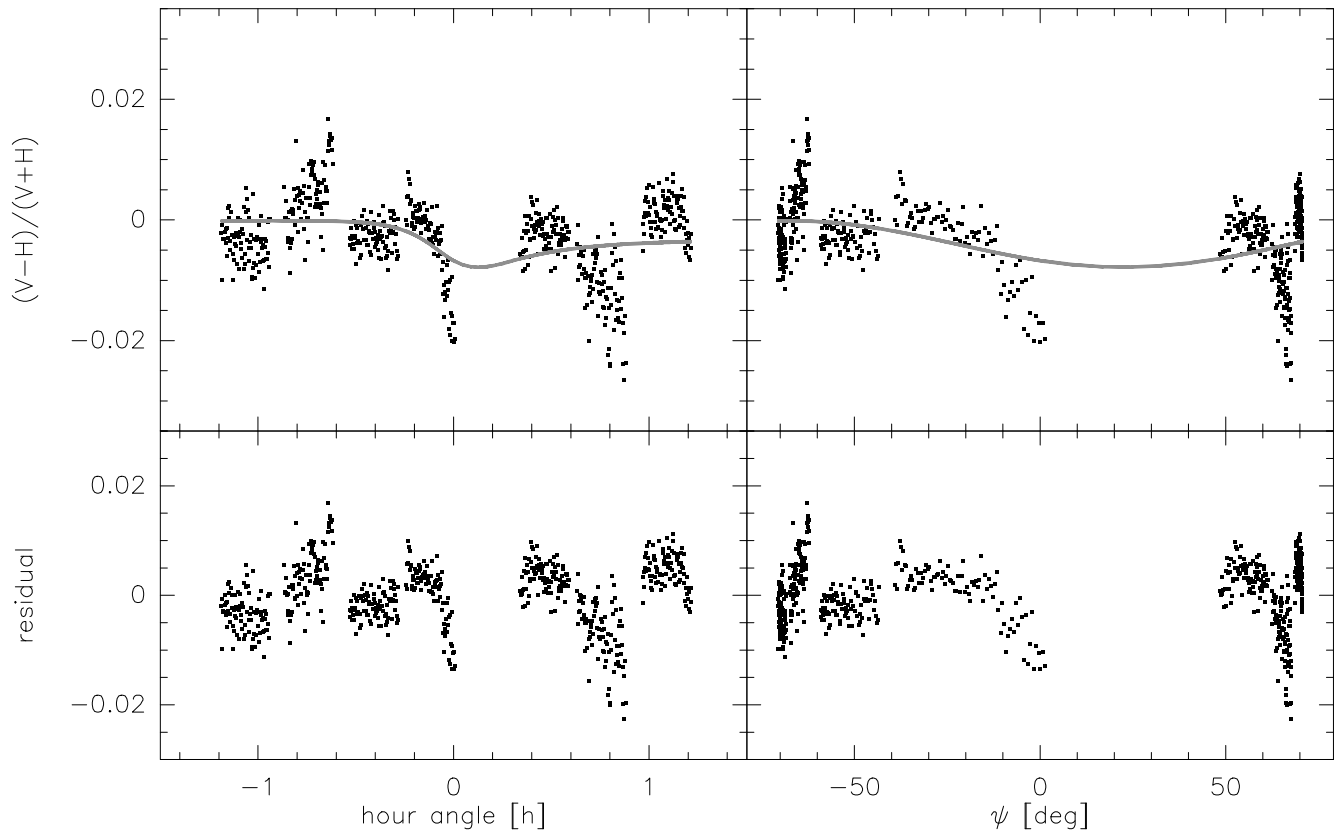


Figure 2. Polarization analysis for 239 GHz flux data. The top panels show $q = (V - H)/(V + H)$ as function of hour angle (on the left) and parallactic angle ψ (on the right). Points indicate data, grey curves indicate the best-fitting polarization models according to Eq. 2. The bottom panels show the corresponding residuals, meaning the differences between data and best-fitting model curves.

parallactic angle. Therefore we executed all observations in time windows centred on the transit. The PdBI is located at a latitude $l = 44.6^\circ$ and 3C 84 has a declination $\delta = 41.5^\circ$. The parallactic angle ψ as function of hour angle follows the pattern presented in Fig. 1. The extreme values $\psi = \pm 72^\circ$ are located at hour angles ± 1.8 h. The ψ curves varies only very slowly at times more than about one hour before or after the transit. As this leads to a clustering of $q(\psi)$ values around $\psi \approx 70^\circ$ which can distort a fit of our model (Eq. 2) to the data, we actually limit our analysis to hour angles < 1.25 h from the transit, meaning $|\psi| \leq 71^\circ$.

In both observing runs (9 and 11 March 2011) we observed 3C 84 with five of the six antennas of the PdBI. We obtained antenna-based amplitudes and phases from factorization of the complex visibilities (see, e.g., Sect. 7.5 of Fomalont & Perley (1999)). Gaps due to calibration intervals and technical interruptions aside, we stored flux data⁴ from each antenna with time resolutions of one second (corresponding to one dump) for both linear polarizations. We used the PdBI wide-band correlator WideX – which provides a bandwidth of 3.6 GHz – in “continuum mode”, meaning each dump value corresponds to the sum of the flux over the full 3.6 GHz spectral band. In order to minimize the impact of antenna pointing instabilities, we computed for each polarization a combined lightcurve by taking the median over all antennas, leaving us with two lightcurves for the V and H channels. Thereafter,

we binned the flux data in time using a bin size of 10 seconds; this value proved to be a good compromise between dense sampling and low scatter within the lightcurves. Eventually, this procedure left us with 630 and 708 data points per polarization for the 239 GHz and 348 GHz lightcurves (for hour angles within ± 1.25 h around the transit), respectively. From the flux data we computed for each observing run $q(\psi)$ according to Eq. 1. To derive degrees and angles of polarization, we fit the model $q'(\psi)$ to the data by means of a χ^2 minimization algorithm.⁵

3 RESULTS

We present the results of our analysis in Fig. 2 for the 239 GHz data and in Fig. 3 for the 348 GHz data. In both figures we display q as function of parallactic and hour angles, the best-fitting polarization models, and the residuals left when subtracting the models from the data. An obvious feature of the q curves are occasional gaps of various sizes. Our observing scheme requires short calibration intervals every ≈ 15 minutes. Interruptions occurring at or closely around the transit cause substantial gaps in ψ coverage even if they are short in terms of observing time (compare Fig. 1); this is evident in both datasets.

⁴ We processed the amplitudes separately, in order not to be affected by atmospheric phase fluctuations. Ignoring the phase information is possible because 3C 84 is a point source for the PdBI.

⁵ Throughout this article, χ always denotes the polarization angle, whereas χ^2 always denotes the weighted sum of the squares of the differences between data and model. This is an unfortunate collision of common nomenclature standards.

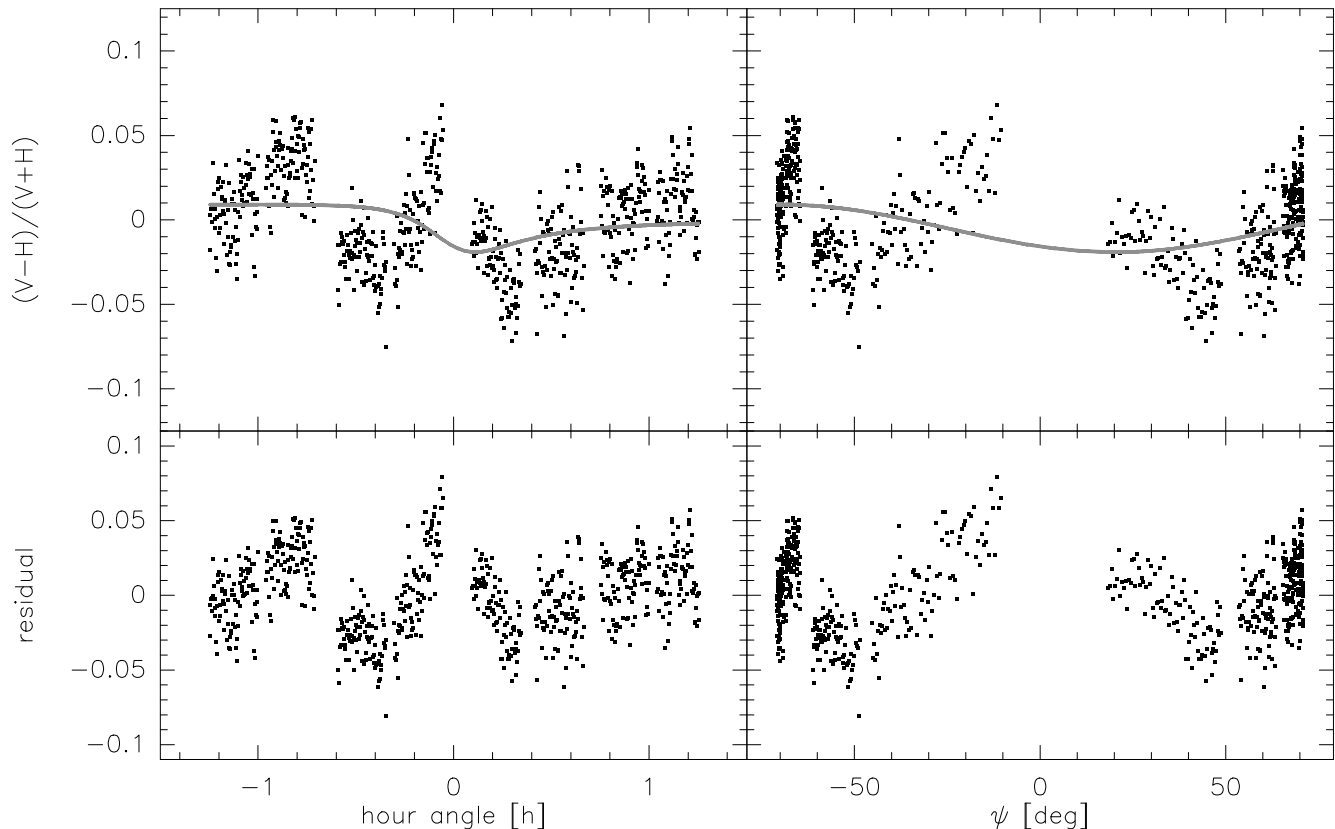


Figure 3. Like Fig. 2 albeit for 348 GHz flux data.

At 239 GHz, we measured antenna temperatures $T_A \approx 159$ mK, translating into a flux density $S_\nu \approx 6.6$ Jy for 3C 84 when adopting a conversion factor of $\rho = 41$ Jy K $^{-1}$. For 1 second of integration time, the statistical measurement uncertainty of the antenna temperature was $\delta T_A = 2.9$ mK, corresponding to a relative uncertainty $\delta T_A/T_A \approx 2\%$. At 348 GHz, we observed $T_A \approx 71$ mK, translating into $S_\nu \approx 4.1$ Jy when adopting a conversion factor of $\rho = 57$ Jy K $^{-1}$. The statistical measurement uncertainty was $\delta T_A = 7.2$ mK, corresponding to a relative uncertainty $\delta T_A/T_A \approx 10\%$.

The accuracy of our observations is limited by systematic uncertainties. In both datasets (Figs. 2 and 3) occasional jumps and drifts show up that have amplitudes substantially larger than the random scatter caused by thermal noise. The principal reason for these systematic deviations are pointing instabilities of the PdBI antennas. The PdBI antennas have pointing accuracies of ≈ 2 – $5''$ depending on antenna orientation, quality of the observation of the required reference point source, and weather conditions. An additional complication was provided by the declination of 3C 84 which is 41.5° . The PdBI is located at a latitude of 44.6° , meaning a transit elevation angle of 86.9° . As the mechanical elevation limit for the PdBI antennas is 87° , we operated the observatory at the very edge of its mechanical tolerances. The beam width (full width at half maximum) of a PdBI antenna is $\approx 17''$ at 239 GHz and $\approx 12''$ at 348 GHz. Accordingly, pointing deviations by few seconds of arc cause substantial fluctuations in the recorded fluxes. In addition, small pointing differences between the receivers for V and H polarizations artificially create a Stokes $Q \equiv V - H \neq 0$. For Gaussian beam profiles, a misalignment of the V and H pointing angles by 10% (20%) of the full width at half maximum of the telescope

beam corresponds to $|Q|/I \approx 2\%$ ($|Q|/I \approx 5\%$). These numbers are maximum values assuming that either V or H is pointed “perfectly” on the target; the actually observed signal depends on telescope orientation and pointing stability. Indeed our observed q curves show excursions of up to approximately $\pm 2\%$ and $\pm 5\%$ at 239 GHz and 348 GHz, respectively. This indicates a V-vs-H alignment uncertainty of $\approx 2''$.

We fit our polarization model $q'(\psi)$ to the data by means of a χ^2 minimization algorithm. We find degrees of polarization $m_L = 0.39 \pm 0.04\%$ and $m_L = 1.4 \pm 0.2\%$ for the 239 GHz and 348 GHz data, respectively. Errors are statistical. Formally, this corresponds to detections of polarizations on levels ≈ 7 – 9σ which would be highly significant. However, inspection of the residuals indicates a poor agreement of model and data. Therefore we address the significance of the presence (or absence) of a polarization signal by means of an F-test (e.g., Müller (1975)). An F-test can be used to compare two models applied to the same dataset and to decide if one of them is significantly better than the other. The two models we explore are (1) our polarization model Eq. 3 (model “P”) and (2) a “null” model that assumes that the data are intrinsically constant (model “0”). For both models we calculate the $\chi^2 \equiv \chi^2/\text{dof}$ (reduced χ^2) of the best fits and from this the parameter

$$f = \frac{\chi_P^2}{\chi_0^2} \quad (4)$$

where f follows an F distribution. The difference between two models is statistically significant on a level s if $f = F_{m,n,s}$. Here m, n are the degrees of freedom for the models “P” and “0”, respectively; s is the significance where $s = 1 - p$ for a false alarm

probability p . From our analysis we find

$$\begin{aligned} f &\equiv F_{627,629,s} = 1.1965 \text{ at } 239 \text{ GHz,} \\ f &\equiv F_{705,707,s} = 1.1362 \text{ at } 348 \text{ GHz.} \end{aligned}$$

These values translate into significance levels – given in fractions as well as Gaussian σ – of

$$\begin{aligned} s &= 98.8\% \equiv 2.5\sigma \text{ at } 239 \text{ GHz,} \\ s &= 95.5\% \equiv 2.0\sigma \text{ at } 348 \text{ GHz.} \end{aligned}$$

Evidently, false alarm probabilities larger than 1%, corresponding to significance levels $\lesssim 2.5\sigma$ in Gaussian terms, indicate that the difference between models “P” and “0” is insignificant. We therefore conclude that we have not (yet) detected linear polarization signals in our data. Accordingly, we quantify our results by quoting 3σ upper limits on the degrees of polarization. These limits are given by the m_L values formally derived from the model fits plus three times their statistical errors. The resulting upper limits on m_L are

$$\begin{aligned} m_L &< 0.5\% \text{ at } 239 \text{ GHz,} \\ m_L &< 1.9\% \text{ at } 348 \text{ GHz.} \end{aligned}$$

Obviously, the model fit results for the polarization angles χ are irrelevant.

4 DISCUSSION

Our observations aimed at the analysis of linear polarization in 3C 84 at observed frequencies of 239 GHz and 348 GHz, corresponding to rest-frame frequencies ν_0 of 243 GHz and 354 GHz, respectively. Our study complements the observations by Trippe et al. (2010) that found $m_L < 1.5\%$ at an observed frequency of 227 GHz. Accordingly, our study expands the frequency range probed by a factor 1.5, corresponding to a factor 2.3 in λ^2 .

Our observations do not find any indication for linear polarization up to rest-frame frequencies of 354 GHz. In theory, synchrotron emission is highly polarized: for the case of 3C 84 with a spectral mm/radio slope – defined via $S_\nu \propto \nu^{-\alpha}$, with S_ν being the flux density – of $\alpha \approx 0.5$ (Trippe et al. (2011)), one may expect degrees of linear polarization of $\approx 69\%$ and $\approx 12\%$ for emission from optically thin and optically thick regions, respectively (e.g., Ginzburg & Syrovatskii (1965); Pacholczyk (1970)). However, these values assume synchrotron emission from homogeneous and isotropic ensembles of electrons moving in uniform magnetic fields. This is an idealization that does not describe properly the situation in AGN that have complex magnetic field structures. In addition, observations suffer from resolution effects: single-dish observations average polarized emission from different source components, leading to “beam depolarization”. Accordingly, the typical linear polarization from AGN found at radio frequencies is about 5% (Altschuler & Wardle (1976; 1977); Aller et al. (1985); Nartallo et al. (1998); Trippe et al. (2010); Agudo et al. (2010)).

The very low level of linear polarization in 3C 84 appears to be connected to the parsec-scale environment of 3C 84 as well as its geometry. Radio-interferometric maps (VLBA, VLBI) show three main source components: a luminous core, a jet extending about 5 pc (in projection) to the south, and a counter-jet extending about 3 pc (in projection) to the north (e.g., Walker & Anantharamaiah (2003), especially their Fig. 1). The southern jet is directed toward

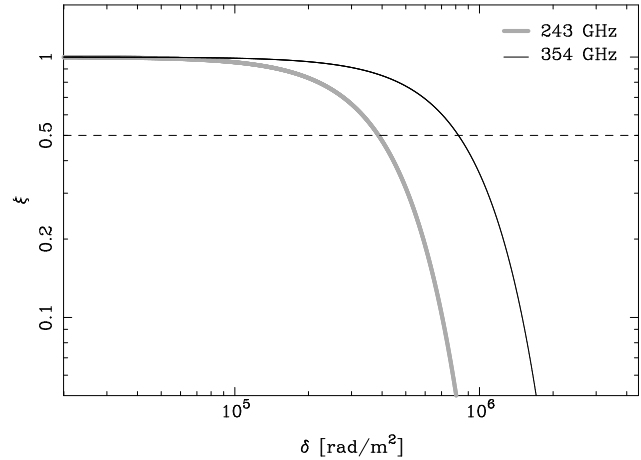


Figure 4. Depolarization parameter ξ as function of RM dispersion δ according to Eq. 8. The grey and black curves indicate the relations for rest-frame frequencies of 243 GHz and 354 GHz, respectively. The horizontal dashed line marks the regime of “substantial” depolarization, here taken to be $\xi \leq 0.5$.

the observer, the northern counter-jet is directed away. The entire galactic nucleus is embedded into dense ionized gas that can act as a Faraday screen (e.g., Heckman et al. (1989)). In addition, the core and the northern jet are located within or behind ionized gas associated with an accretion disk (Walker et al. (2000)).

Our observations provide new information on the physical properties of the Faraday screen located in front of the source. Linearly polarized radiation passing through a magnetized plasma experiences Faraday rotation. This means the intrinsic polarization angle χ is modified like $\chi \rightarrow \chi' = \chi + \Delta\chi$, with

$$\Delta\chi = \text{RM} \times \lambda_0^2. \quad (5)$$

Here λ_0 is the rest-frame wavelength and RM is the rotation measure

$$\frac{\text{RM}}{\text{rad m}^{-2}} = 8.1 \times 10^5 \int_{\text{l.o.s.}} \left(\frac{B_{\parallel}}{\text{G}} \right) \left(\frac{n_e}{\text{cm}^{-3}} \right) d \left(\frac{l}{\text{pc}} \right), \quad (6)$$

with B_{\parallel} being the strength of the magnetic field parallel to the line of sight (l.o.s.), n_e being the electron number density, and l being the coordinate directed along the l.o.s. (e.g., Rybicki & Lightman (1979); Wilson, Rohlfs & Hüttemeister (2010)). If RM shows modulations with amplitudes ΔRM on spatial scales smaller than the source, the source radiation experiences different Faraday rotation depending on the position in the plane of the sky. Observations that do not resolve the RM structure spatially superimpose electric field vectors with different orientations. This partially averages out the polarization signal, reducing the degree of polarization observed.

Quantitatively, we may understand the strong depolarization of 3C 84 by describing the Faraday screen as “Faraday thick” (e.g., Brentjens & de Bruyn (2005)). From Eq. 5 it is evident that a medium is Faraday thick if

$$\Delta\text{RM} \times \lambda_0^2 \gg 1. \quad (7)$$

Our observations are obtained at wavelengths as short as $\lambda_0 = 0.85$ mm. Accordingly, we require $\Delta\text{RM} \gg 10^6$ rad m⁻² for efficient depolarization.

A more sophisticated calculation is possible when assuming that the RM fluctuations follow a Gaussian distribution with dispersion $\delta \approx \Delta\text{RM}$. If the source is not resolved spatially, one finds the depolarization law

$$\xi = \exp\left(-2\delta^2\lambda_0^4\right) \quad (8)$$

(Burn (1966); Tribble (1991)). The parameter $\xi \in [0, 1]$ is the ratio of observed and intrinsic degree of linear polarization. We present ξ as a function of δ in Fig. 4 for the rest-frame frequencies of 243 GHz and 354 GHz, corresponding to rest-frame wavelengths of 1.23 mm and 0.85 mm, respectively. Evidently, it is possible to derive δ if ξ is known for a given rest-frame wavelength. However, this requires information on the intrinsic polarization of 3C 84 that is not available. Instead, we have to restrict ourselves to the statement that we observe “substantial” depolarization at wavelengths as short as 0.85 mm. When defining substantial depolarization as $\xi \leq 0.5$, we are able to derive $\delta \gtrsim 4 \times 10^5 \text{ rad m}^{-2}$ and $\delta \gtrsim 8 \times 10^5 \text{ rad m}^{-2}$ at 243 GHz and 354 GHz, respectively. In agreement with the crude estimate from Eq. 7, we see indication for $\Delta\text{RM} \approx 10^6 \text{ rad m}^{-2}$ and, accordingly, $|\text{RM}| \gtrsim 10^6 \text{ rad m}^{-2}$.

Our estimate of RM makes it possible to probe the physical conditions in the parsec-scale environment of 3C 84 by means of Eq. 6. For $|\text{RM}| \gtrsim 10^6 \text{ rad m}^{-2}$, we find $\langle B_{\parallel} n_e l \rangle \gtrsim 1$, with $\langle \dots \rangle$ indicating the line-of-sight average of the enclosed expression. As pointed out by Taylor et al. (2006), the effective line-of-sight extension of the Faraday screen can be estimated to $l \approx 10 \text{ pc}$. As for assessing the electron density, we have to address the various components that contribute. First, the particle density on spatial scales $\lesssim 4 \text{ kpc}$ has been found to be $n_e \approx 270 \text{ cm}^{-3}$ based on optical spectroscopy of [S II] lines (Heckman et al. (1989)). Second, for the immediate vicinity ($\lesssim 5 \text{ pc}$) of the core and the northern counter-jet densities $n_e \gtrsim 2000 \text{ cm}^{-3}$ have been derived from radio continuum spectroscopy (O’Dea, Dent & Balonek (1984); Walker & Anantharamaiah (2003)). Overall, we may assume an average particle density on the order of $n_e \approx 1000 \text{ cm}^{-3}$, in agreement with particle densities commonly found in the narrow line regions of Seyfert galaxies (e.g., Koski (1978); Bennert et al. (2006)). From the combined information on l and n_e we conclude on the presence of magnetic fields with $B_{\parallel} \gtrsim 100 \mu\text{G}$.

Even though the values we derive for RM and B_{\parallel} are fairly high, they are by no means extraordinary. Values of $|\text{RM}| \approx 5 \times 10^5 \text{ rad m}^{-2}$ can be seen also in the radio nucleus of the Seyfert 1 galaxy 1637+574 (Trippe et al. (2012)) and, most notably, in the Galactic centre radio source Sagittarius A* (Marrone et al. (2006); Macquart et al. (2006)). Magnetic fields with $B_{\parallel} \approx 100 \mu\text{G}$ are compatible to those found in the centre of the Milky Way, where field strengths in the range $\approx 100 \mu\text{G} - 1 \text{ mG}$ have been reported (e.g., Morris & Yusef-Zadeh (1989); Ferrière (2009), and references therein). Accordingly, the parsec-scale environment of 3C 84 is not unusual with respect to the values of its parameters n_e and B_{\parallel} but – if at all – with respect to its spatial variability as seen in projection. The total extension of the radio source is $\lesssim 10 \text{ pc}$, and observations have resolved structure on scales less than one parsec (e.g., Krichbaum et al. (1992); Taylor et al. (2006)). Accordingly, RM fluctuations with amplitudes on the order of $\Delta\text{RM} \approx 10^6 \text{ rad m}^{-2}$ have to occur – in projection – on spatial scales $\lesssim 1 \text{ pc}$ in order to warrant efficient depolarization. This may partially be caused by the fact that observations are affected by contributions from at least two components of interstellar matter with potentially different matter distributions and magnetic field geometries: the foreground ionized gas and the gas associated with the accretion disk. This would also be consistent with the observations by Taylor et al. (2006); they observed some localized linear polarization in the jet moving toward the observer with an apparent expansion velocity of $\approx 0.5c$ (e.g., Asada et al. (2006)), i.e. from a source component that would be

less affected by an accretion disk and that could have penetrated the Faraday screen partially.

A priori, we may expect some loss of linear polarization by Faraday conversion from linear to circular polarization (e.g., Jones (1988)). From single-dish observations, degrees of circular polarization from $m_C \approx 0.2\%$ at 4.8 GHz (Aller et al. (2003)) up to $m_C \approx 0.5\%$ at 86 GHz (Agudo et al. (2010)) have been reported. VLBA imaging at angular resolutions of $\approx 0.8 \text{ mas}$ unveils localized circular polarization in the core with $m_C \approx 3\%$ at 15 GHz (Homan & Wardle (2004)). In addition, Homan & Wardle (2004) find for the core polarization $m_C \propto \nu^{-0.9}$; accordingly, polarization levels of $m_C \lesssim 0.3\%$ may be expected at frequencies $\gtrsim 239 \text{ GHz}$. From the combined circular polarization information available, we conclude that Faraday conversion contributes only marginally to the loss of linear polarization.

5 SUMMARY AND CONCLUSIONS

We report the results of a search for linear polarization in the active nucleus of the Seyfert 2 galaxy 3C 84. Observations were carried out with the IRAM Plateau de Bure Interferometer at observatory-frame frequencies of 239 GHz and 348 GHz, corresponding to rest-frame frequencies of 243 GHz and 354 GHz. We applied Earth rotation polarimetry as the principal tool of analysis. Our study arrives at the following conclusions:

- (i) We do not detect linear polarization. Our analysis finds 3σ upper limits on the degree of polarization of 0.5% and 1.9% at 239 GHz and 348 GHz, respectively.
- (ii) Faraday conversion from linear to circular polarization can be expected on levels of $\lesssim 0.3\%$. Accordingly, this mechanism provides only a marginal contribution to the loss of linear polarization observed.
- (iii) Assuming depolarization by a local Faraday screen, we constrain the rotation measure, as well as the fluctuations therein, to be $\gtrsim 10^6 \text{ rad m}^{-2}$. From this we estimate line-of-sight magnetic field strengths of $\gtrsim 100 \mu\text{G}$. These values are fairly high but consistent with observations of other galactic nuclei, most notably the centre of the Milky Way.
- (iv) Given the physical dimensions of 3C 84 and its observed structure, the Faraday screen appears to show prominent small-scale structure, with $\Delta\text{RM} \gtrsim 10^6 \text{ rad m}^{-2}$ on projected spatial scales $\lesssim 1 \text{ pc}$.

Our study underlines the power of polarization observations for studies of the parsec-scale environment of 3C 84 in special and AGN in general. In order to further probe the Faraday screen of 3C 84, it will be necessary to obtain observations that actually detect linear polarization on levels $> 1\%$. Accordingly, observations at ever higher frequencies, well into the sub-mm/radio regime, should be done. In addition, high-resolution radio interferometric mapping, e.g. with the Global Millimetre-VLBI Array (GMVA), may resolve localized polarized structure and provide new insights into local physical conditions.

ACKNOWLEDGMENTS

We are grateful to the entire PdBI team for carrying out the observations and technical support. The data analysis made use of the GILDAS software package (<http://www.iram.fr/IRAMFR/GILDAS/>)

developed and maintained by the GILDAS team. We also applied the software package DPUSER (<http://www.mpe.mpg.de/~ott/dpuser/index.html>) developed and maintained by Thomas Ott at MPE Garching.

REFERENCES

- Asada K., et al. 2006, PASJ, 58, 261
 Agudo I., et al. 2010, ApJSS, 189, 1
 Aller H.D., et al. 1985, ApJSS, 59, 513
 Aller H.D., Aller M.F., Plotkin R.M. 2003, ApSS, 288, 17
 Altschuler D.R., Wardle J.F.C. 1976, MNRAS, 82, 1
 Altschuler D.R., Wardle J.F.C. 1977, MNRAS, 179, 153
 Beltrán M.T., et al. 2004, A&A, 416, 631
 Bennert N., et al. 2006, A&A, 459, 55
 Brentjens M.A., de Bruyn A.G. 2005, A&A, 441, 1217
 Burn B.J. 1966, MNRAS, 133, 67
 Dreher J.W., Carilli C.L., Perley R.A. 1987, ApJ, 316, 611
 Ferrière K. 2009, A&A, 505, 1183
 Fomalont E.B., Perley R.A. 1999, in: Taylor G.B., et al. (eds.), ASP Conf. Ser. 180, 79
 Ginzburg V.L., Syrovatskii S.I. 1965, ARA&A, 3, 297
 Heckman T.M., et al. 1989, ApJ, 338, 48
 Homan D.C., Wardle J.F.C. 2004, ApJ, 602, L13
 Jones T.W. 1988, ApJ, 332, 678
 Kembhavi A.K., Narlikar J.V. 1999, Quasars and Active Galactic Nuclei, Cambridge Univ. Press, Cambridge
 Koski A.T. 1978, ApJ, 223, 56
 Krichbaum T.P., et al. 1992, A&A, 260, 33
 Krolik J.H. 1999, Active Galactic Nuclei, Princeton Univ. Press, Princeton
 Lister M.L., et al. 2009, AJ, 137, 3718
 Macquart J.-P., et al. 2006, ApJ, 646, L111
 Marrone D.P., et al. 2006, 640, 308
 Morris M., Yusef-Zadeh F. 1989, ApJ, 343, 703
 Müller P.H. 1975, Lexikon der Wahrscheinlichkeitsrechnung und Mathematischen Statistik, Akademie-Verlag, Berlin
 Nartallo R., et al. 1998, MNRAS, 297, 667
 O'Dea C.P., Dent W.A., Balonek T.J. 1984, ApJ, 278, 89
 Pacholczyk A.G. 1970, Radio Astrophysics, W.H. Freeman & Co.
 Rybicki G.B., Lightman A.P. 1979, Radiative Processes in Astrophysics, Wiley-VCH, Weinheim
 Saikia D.J., Salter C.J. 1988, ARA&A, 26, 93
 Sault R.J., Hamaker J.P., Bregman J.D. 1996 A&AS, 117, 149
 Taylor G.B., et al. 2006, MNRAS, 368, 1500
 Thompson A.R., Moran J.M., Swenson G.W. 2001, Interferometry and Synthesis in Radio Astronomy, 2nd edn., Wiley-VCH, Weinheim
 Tribble P.C. 1991, MNRAS, 250, 726
 Trippe S., et al. 2010, A&A, 515, A40
 Trippe S., et al. 2011, A&A, 533, A97
 Trippe S., et al. 2012, A&A, 540, A74
 Walker R.C., et al. 2000, ApJ, 530, 233
 Walker R.C., Anantharamaiah K.R. 2003, AJ, 125, 1756
 Wilson T.L., Rohlfs K., Hüttemeister S. 2010, Tools of Radio Astronomy, 5th edn., Springer, Berlin
 Winters J.M., Neri R. 2011, An introduction to the IRAM Plateau de Bure Interferometer, IRAM manual, version 4.2-00

This paper has been typeset from a \TeX / \LaTeX file prepared by the author.